Applied Catalysis B: Environmental 305 (2022) 121025

Contents lists available at ScienceDirect

Applied Catalysis B: Environmental

journal homepage: www.elsevier.com/locate/apcatb

Afterglow-catalysis and molecular imprinting: A promising union for elevating selectivity in degradation of antibiotics

Ye Zhang [a,1], Zheng-Wu Wang [a,1], Xiao-Ting Yang [a], Yi-Zhou Zhu [b,*], He-Fang Wang [a,*]

[a] Research Center for Analytical Sciences, College of Chemistry, Nankai University, Tianjin Key Laboratory of Biosensing and Molecular Recognition, Tianjin 300071, China

[b] State Key Laboratory and Institute of Elemento-Organic Chemistry, Nankai University, Tianjin 300071, China

ARTICLE INFO

Keywords:
Afterglow-catalysis
Molecular imprinting
Persistent luminescence nanoparticles
Antibiotics
Photoluminescence self-report

ABSTRACT

We propose a novel design for smart-catalyst to selective degrade antibiotics and self-report degradation process by combining molecular-imprinting (MI) and afterglow-catalysis. Tetracycline (TC) is used as imprinted template, and $ZnGa_2O_4$ doped with Cr^{3+} (ZGO) is for catalytic degradation even in-the-dark. TC-involved direct hydrothermal-growth of ZGO at 60/80 °C gives MI-ZGO, followed by 750 °C-calcination, and then ethylenediaminetetraacetic-acid (EDTA) etching to get MI-ZGO-750-EDTA. The imprinting mechanism and effect of temperature of MI-ZGO growth on degradation are investigated. The imprinting factor (IF), adsorption/degradation ratio between MI-ZGO-750-EDTA and non-imprinted NI-ZGO-750-EDTA, is used to evaluate the selectivity of three degradation modes (day-and-night, afterglow-catalysis and photo-catalysis). The highest selectivity of 60-MI-ZGO-750-EDTA is gained in afterglow-catalytic degradation, wherein IF of TC is 3 times of oxytetracycline (OTC) and 3.5 times of malachite green (MG) in pure-solutions, while in mixed-solutions, IF of TC is 3.5 times of OTC and 5.2 times of MG. Besides, photoluminescence of MI-ZGO-750-EDTA can self-report degrading process.

1. Introduction

The abuse and random discharge of antibiotics promote the continuous proliferation of drug-resistant genes, and thus endanger the health of humans and other organisms. Accordingly, the selective degradation of the environmental antibiotics has been the important issue of ecological security [1–4]. Multifarious methods, such as advanced oxidation [5–7], biological treatment [8–10] and photocatalytic degradation [11–18], have been explored for degradation of antibiotics. However, most degradation has poor selectivity, that is, the substance with higher concentration degrades first, while the toxic antibiotics with lower concentration cannot be degraded effectively. Actually, the toxicity is not proportional to the concentration, even the overall toxicity depends on a small proportion of refractory antibiotics [19–21]. Therefore, to create the strategy for selective degradation towards specific antibiotics is vital to eliminate the negative effect of antibiotics on environmental safety.

Molecular imprinting (MI) is a widely-used method for getting the selective recognition of the imprinted templates, wherein the templates are first imprinted into the substrates, and then remove of the templates leaves the special cavities perfectly matching the shape, size and functional groups with the templates [22–28]. The combination of photocatalysts (usually semiconductors) with MI endows the photocatalysts with capability of selective catalytic degradation [29–31], for instance, the MI-TiO_2 and MI-ZnO have been used as the photocatalysts of selective degradation [32–36]. Although the photocatalytic degradation under sunlight radiation is an environmental-friendly and popular method, the over-dependence of photocatalysts on in-situ lighting limits the applications in the dark or bad-weather condition. The afterglow-catalytic degradation just makes up for that, therein the catalytic degradation still works for a period after the light irradiation is ceased [37]. Besides, afterglow-catalytic degradation avoids the light-scattering by the catalysts and thus enable the usage of large amount of catalysts, and guarantee the degradation at deep depth [38]. To the best of our knowledge, there is no report combining MI with afterglow-catalysis to achieve the selective around-the-clock degradation of antibiotics.

Herein, we propose the selective catalytic degradation of antibiotics

* Corresponding authors.
E-mail addresses: zhuyizhou@nankai.edu.cn (Y.-Z. Zhu), wanghefang@nankai.edu.cn (H.-F. Wang).
[1] Contribute equally

https://doi.org/10.1016/j.apcatb.2021.121025
Received 25 October 2021; Received in revised form 14 December 2021; Accepted 19 December 2021
Available online 21 December 2021

by molecularly imprinted Cr^{3+}-doped $ZnGa_2O_4$ ($ZnGa_2O_4$:Cr^{3+}, ZGO). Scheme 1 illustrates the diagram, wherein ZGO, the semiconductors with fine afterglow property [39–42], has the capability of catalytic degradation of pollutants in-the-dark and photoluminescence (PL)-self-reporting the pollutants degradation [37]; and tetracycline (TC), a typical antibiotic widely used and being listed as the toxic pollutants [43–45], is explored as the imprinted template. The molecularly imprinted ZGO (MI-ZGO) was simply synthesized via one-pot growth of ZGO in the presence of TC template, then calcination at 750 °C to remove the TC template and elevate the PL and afterglow, and finally EDTA-etching for generating more oxygen vacancy and improving the water-dispersibility. The final product was marked as MI-ZGO-750-EDTA, and the parallelly-synthesized non-imprinted ZGO was signed as NI-ZGO-750-EDTA. The synthesis conditions and TC imprinting mechanism are systematically investigated. The adsorption, day-and-night, photo- and afterglow-catalytic degradation of TC by MI-ZGO-750-EDTA and NI-ZGO-750-EDTA were compared, and degradation of TC and interferences were determined by UV–vis absorption or high-performance liquid chromatography (HPLC) of the supernatants. The degradation process was also evaluated by ZGO PL self-reporting. The proposed MI-ZGO-750-EDTA has both the functions of selective catalytic degradation toward TC and PL-self-reporting TC degradation, and displays the greatly-elevated selectivity and robust anti-interference in afterglow-catalytic degradation. This work provides a new and effective solution on how to selectively degrade the antibiotics or other pollutants with low-concentration but high-toxicity in both cases of photo-irradiation and in-the-dark.

2. Experimental section

2.1. Reagents and apparatus

All reagents and apparatus used in the experiments are listed in Supporting Information (SI).

2.2. Preparation of MI/NI-ZGO-750-EDTA

In a typical procedure, $Zn(NO_3)_2{\cdot}6\ H_2O$ (5 mmol), $Ga(NO_3)_3$ solution (0.4 M, 25 mL) and $Cr(NO_3)_3$ solution (0.02 M, 1 mL) were added into 130 mL ultrapure water. The mixture was stirred to get the clear solutions, and *t*-butylamine was added dropwise till pH of that mixture reached 8. After that, TC (0.5 mmol) was added, and the resultant mixture was fully sonicated, and stirred for 1 h at room temperature, and then transferred into 25 mL Teflon-lined stainless-steel autoclaves and heated at 60 °C or 80 °C for 16 h. After cooling to room temperature, the mixtures were centrifuged, and the precipitates were washed with water twice and ethanol once, and then dried in vacuum for 12 h. The obtained products were marked as 60-MI-ZGO and 80-MI-ZGO respectively. The corresponding products after calcination in air at 750 °C for 1 h were marked as 60-MI-ZGO-750 and 80-MI-ZGO-750 respectively (500 and 1000 °C calcination was also examined, and finally 750 °C was selected). The EDTA-etching procedure was the same as our previous publication [46], and the resultant products were marked as 60-MI-ZGO-750-EDTA and 80-MI-ZGO-750-EDTA respectively. The non-imprinted series were synthesized in parallel with the same steps except without adding TC, and marked as the corresponding forms of NI tag.

2.3. Selective adsorption and day-and-night degradation of TC by MI/NI-ZGO-750-EDTA

Typically, suitable amount of MI-ZGO-750-EDTA were settled in quartz tube and kept in dark for 12 h, and then TC solution was added into, to make 35 mL homogeneous suspensions with initial concentration of MI-ZGO-750-EDTA (0.25, 0.5, 0.75 and 1.0 $g{\cdot}L^{-1}$) and TC (25 $mg{\cdot}L^{-1}$), and this time point was marked as "start". The suspensions were kept stirring in a lamp-house, first adsorption in-the-dark for 1 h, and then with irradiation by 500 W Xe-lamp (with 420 nm filter) for 2 h (degradation in day), and then in-the-dark for 4 h (degradation at night). The TC concentration was determined via the UV–vis absorbance (at 359 nm) of supernatants from centrifuging the suspensions at "start, in dark 1 h, Xe 2 h, and in dark 4 h". The concentration of catalyst was optimized by using 60/80-MI-ZGO-750-EDTA as the catalysts, and 0.75 $g{\cdot}L^{-1}$ was chosen as the best. The imprinting effect of TC adsorption and degradation was evaluated by comparison between MI-ZGO-750-EDTA and the corresponding NI-ZGO-750-EDTA. The concentration of TC in pure TC solution under Xe lamp (with 420 nm filter) irradiation were used as the control for evaluation of TC degradation.

Oxytetracycline (OTC), one of the structure analogues of TC, was used for comparing the imprinting selectivity. All experiments were done with 60-MI/NI-ZGO-750-EDTA by the same operation as TC. For selectivity evaluation in mixed solution of TC/OTC, the concentration was determined by HPLC (details in SI).

2.4. Anti-interference of TC degradation by MI-ZGO-750-EDTA

To evaluate the anti-interference of selective TC degradation, OTC and malachite green (MG), were used as the interferences. The afterglow-catalytic degradation of TC, OTC, MG, or mixture of TC/OTC, TC/MG by 60-MI/NI-ZGO-750-EDTA was evaluated and compared. For the afterglow-catalytic degradation, the homogeneous dispersions of 0.75 $g{\cdot}L^{-1}$ of 60-MI/NI-ZGO-750-EDTA were continuously irradiated for 2 h via a 500-W Xe lamp, and then the lamp was turned off, and MG solution (50 $mg{\cdot}L^{-1}$), TC or OTC solution (25 $mg{\cdot}L^{-1}$) or the mixture of MG/TC (50 / 25 $mg{\cdot}L^{-1}$), OTC/TC (25 / 25 $mg{\cdot}L^{-1}$) solutions were added into that dispersion respectively, and then the resultant mixtures

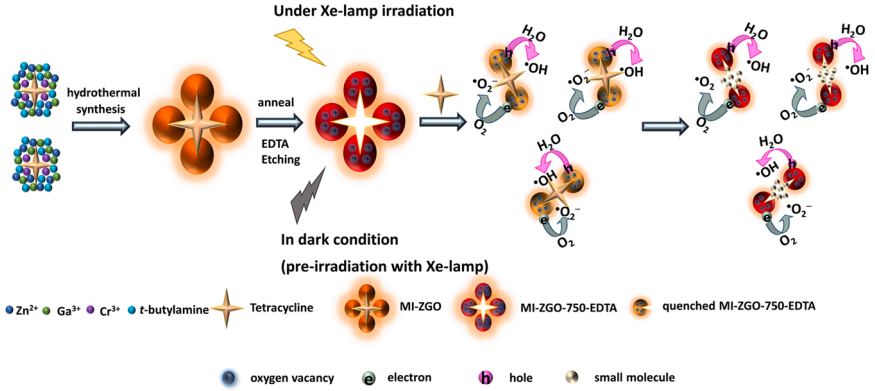

Scheme 1. The schematic diagram about the synthesis of MI-ZGO-750-EDTA and the functions of TC selective afterglow-catalytic degradation and PL-self-reporting TC degradation.

were kept stirring in-the-dark for 4 h. For photo-catalytic degradation, the homogeneous dispersions of 0.75 $g{\cdot}L^{-1}$ of 60-MI/NI-ZGO-750-EDTA in the presence of MG solution (50 $mg{\cdot}L^{-1}$), TC or OTC solution (25 $mg{\cdot}L^{-1}$) or the mixture of MG/TC (50 / 25 $mg{\cdot}L^{-1}$), OTC/TC (25 / 25 $mg{\cdot}L^{-1}$) solutions were continuously irradiated for 4 h via a 500-W Xe lamp (with 420 nm filter). Concentration of TC, OTC and MG after degradation was evaluated by UV–vis absorbance (TC at 359 nm, OTC at 353 nm and MG at 616 nm respectively) and HPLC (for mixed TC/OTC solutions) of the supernatants from centrifuging 2.5 mL mixtures piped out at different intervals.

2.5. PL self-reporting of TC degradation

The monitoring of degrading process was evaluated by the direct measurements of the emission spectra of dispersions piped-out at different intervals (the intensity at 698 nm was used for the quantitative analysis).

3. Results and discussion

3.1. Synthesis of MI-ZGO-750-EDTA and imprinting mechanism

MI-ZGO-750-EDTA was synthesized via three steps (Scheme 1). First MI-ZGO was hydrothermally synthesized by the direct growth of ZGO in

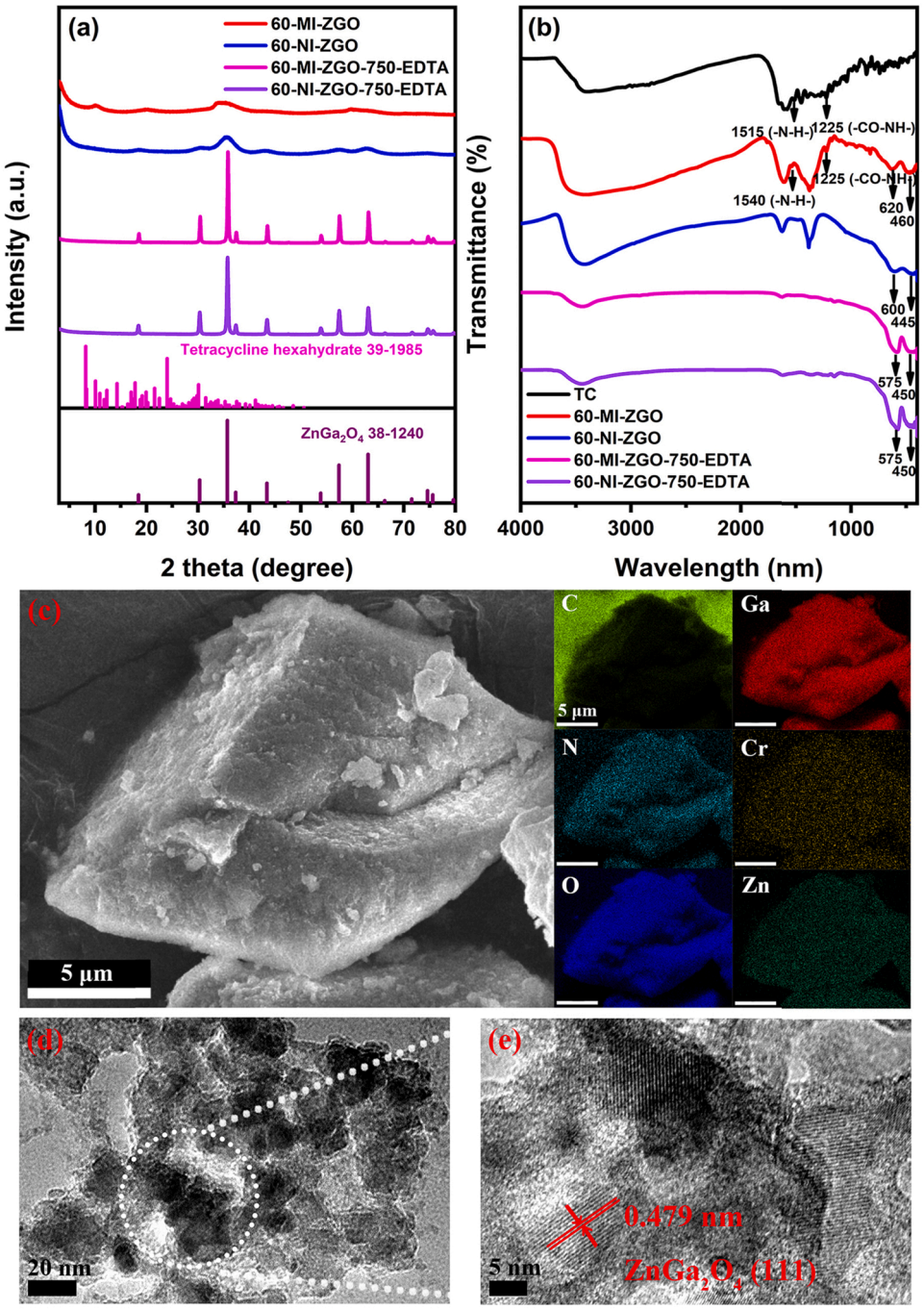

Fig. 1. (a) XRD of 60-MI/NI-ZGO and 60-MI/NI-ZGO-750-EDTA, (b) FT-IR of TC, 60-MI/NI-ZGO and 60-MI/NI-ZGO-750-EDTA, (c) SEM images and elemental mapping of 60-MI-ZGO, and (d) TEM and (e) HRTEM of 60-MI-ZGO.

the presence of TC template, and then MI-ZGO was calcined at 750 °C to get MI-ZGO-750, and finally MI-ZGO-750 was etched by EDTA to get MI-ZGO-750-EDTA. The different calcination temperature is examined, low temperature of 500 °C leads to poor afterglow and incomplete removal of TC template, while high temperature of 1000 °C results in the collapse of imprinting sites of TC and thus poor imprinting effect (Fig. S1 in SI). Consequently, 750 °C was used finally.

We first discuss MI/NI-ZGO. To avoid deformation or carbonization of TC, we tried to synthesize MI-ZGO at 60 or 80 °C. The imprinting of TC into ZGO was proved by X-ray powder diffraction (XRD), Fourier transform Infrared spectra (FT-IR), scanning electron micrograph (SEM) mapping, and X-ray photoelectron spectra (XPS) analysis of 60-MI/NI-ZGO and 80-MI/NI-ZGO before and after calcination and EDTA etching.

Both 60-MI-ZGO and 60-NI-ZGO have the pure $ZnGa_2O_4$ crystal form

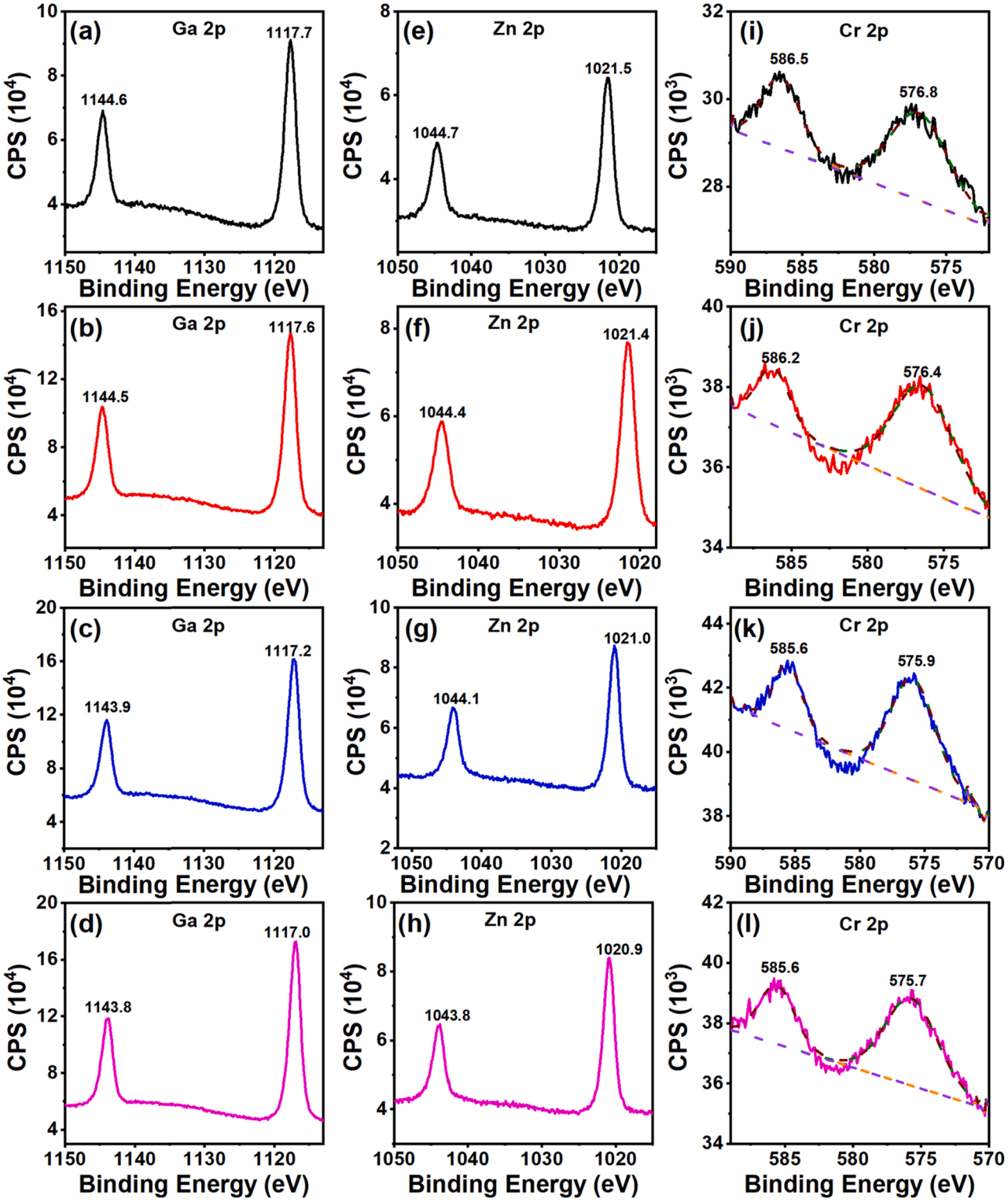

Fig. 2. (a-d) Ga 2p, (e-h) Zn 2p and (i-l) Cr 2p XPS spectra of (a, e, i) 60-MI-ZGO, (b, f, j) 60-NI-ZGO, (c, g, k) 60-MI-ZGO-750-EDTA and (d, h, i) 60-NI-ZGO-750-EDTA.

(JCPDS 38–1240) in the XRD patterns (Fig. 1a), and 60-MI-ZGO exhibits the extra characteristic peak corresponding to TC (JCPDS 39–1985) at low angle range, suggesting the existence of TC and ZGO in 60-MI-ZGO. Besides, the broader diffraction peaks of 60-MI-ZGO over 60-NI-ZGO implies the changes of size and microstructure caused by the interaction between TC and ZGO, which is further proved by FT-IR spectra (Fig. 1b) and XPS spectra (Fig. 2). The obvious red-shifted peaks at 460 and 620 cm^{-1} in 60-MI-ZGO over the peaks at 445 and 600 cm^{-1} in 60-NI-ZGO reveals the interaction between -NH_2 or -OH of TC and Ga^{3+}, Zn^{2+} or Cr^{3+} of ZGO. In addition, compared with 60-NI-ZGO, 60-MI-ZGO has the extra characteristic peaks of -CO-NH- at 1225 cm^{-1} and -N-H- at 1540 cm^{-1}, which are the same as the peaks in FT-IR spectrum of pure TC, also demonstrating the existence of TC in 60-MI-ZGO. The element distribution of Zn, Ga, O, Cr, C, and N in SEM images of 60-MI-ZGO (Fig. 1c) indicates TC is uniformly incorporated into ZGO, and the TEM image of 60-MI-ZGO (Fig. 1d) shows the diameter of ZGO nanoparticles is about 20 nm. The inter-planar spacing of 0.479 nm in HRTEM is corresponding to (111) of ZGO (Fig. 1e), while the amorphous TC around the ZGO nanoparticles does not show an obvious ordered crystalline. The interaction of TC with ZGO is mainly via the binding of hydroxyl or amino group of TC with Ga, Zn and Cr in ZGO, which is proved by the higher binding energies of Ga 2p, Zn 2p, Cr 2p in XPS spectra of 60-MI-ZGO than 60-NI-ZGO (Fig. 2) [35,47,48]. The 80-MI/N-I-ZGO has the same phenomena as 60-MI/NI-ZGO (Fig. S2).

We then discuss MI/NI-ZGO-750-EDTA. Both 60-MI-ZGO-750-EDTA and 60-NI-ZGO-750-EDTA have nearly the same curves of thermogravimetric analysis (Fig. S3), the clean pure $ZnGa_2O_4$ patterns (Fig. 1a), and the same IR absorption peaks corresponding to Ga-O at 450 cm^{-1} and Zn-O at 575 cm^{-1} (Fig. 1b). These data indicate the successful removal of TC template in MI-ZGO-750-EDTA. The obvious blue-shift of the absorption of Ga-O and Zn-O in MI/NI-ZGO-750-EDTA against NI-ZGO is probably ascribed to the structure change from calcination at 750 °C. The binding energies of Ga 2p, Zn 2p and Cr 2p in 60-MI-ZGO-750-EDTA are still 0.1–0.3 eV higher than those in 60-NI-ZGO-750-EDTA, which indicates that although TC has been removed, the recognition sites of TC are still retained on the surface of 60-MI-750-ZGO-EDTA. The XPS O 1 s in 60-MI-ZGO-750-EDTA (Fig. S4) exhibits two signals, one is at 530.0 eV attributing to the lattice oxygen, and the other is at 531.0 eV corresponding to the O atoms coordinated with oxygen defects [46]. The latter suggests the existence of oxygen vacancy in 60-MI-ZGO-750-EDTA.

3.2. Characterization of MI/NI-ZGO-750-EDTA

The SEM (Fig. 3) and TEM (Fig. S5) images display the spherical nanoparticles of MI/NI-ZGO-750-EDTA. The statistical analysis of randomly selected 100 nanoparticles in Fig. 3 elucidates that the size of 60-MI-ZGO-750-EDTA and 60-NI-ZGO-750-EDTA is 49.46 ± 9.14 nm and 31.56 ± 5.38 nm respectively, while the size of 80-MI-ZGO-750-EDTA and 80-NI-ZGO-750-EDTA is 46.74 ± 7.40 nm and 31.23 ± 6.14 nm. That is to say, MI-ZGO-750-EDTA displays the larger particle size than the corresponding NI-ZGO-750-EDTA, which is most probably ascribed to the interaction of TC template with the ions in ZGO. The high-resolution TEM images (HRTEM) (inset in Fig. S5) show the typical (311) lattice lines of pure spinel $ZnGa_2O_4$ of MI/NI-ZGO-750-EDTA.

The prepared MI/NI-ZGO-750-EDTA owns fine afterglow property (Fig. 4a,b), as the afterglow still has high intensity after stoppage of excitation for 1 h. Both 60-MI-ZGO-750-EDTA and 80-MI-ZGO-750-EDTA show the slightly slower decay than the corresponding NI-ZGO-750-EDTA, most probably due to the larger size of MI-ZGO-750-EDTA over the corresponding NI-ZGO-750-EDTA [46] as shown in Fig. 3. But the difference between the afterglow decay of MI and NI is indeed very little, so the subsequent different degradation efficiency of MI- and NI- ZGO-750-EDTA is mainly attributed to the selectivity of TC imprinting, especially in the dark condition.

To evaluate whether the prepared MI/NI-ZGO-750-EDTA meet the energy demand of photo- or afterglow- catalytic degradation, we measured the band gaps of 60-MI/NI-ZGO-750-EDTA via diffuse reflectance spectra (DRS, Fig. 4c), and estimated the potential of conduction band (E_{CB}) and the potential of valance band (E_{VB}) via Mott-Schottky curve (Fig. 4d,e). The Kubelka-Munk plots are drawn preconditioned with the indirect-band-gap semiconductor of $ZnGa_2O_4$, from which the band gap of 60-MI-ZGO-750-EDTA and 60-NI-ZGO-750-EDTA is estimated as 4.15 and 4.08 eV, respectively. The positive slopes in the Mott-Schottky curves (Fig. 4d and e) declare *n*-type

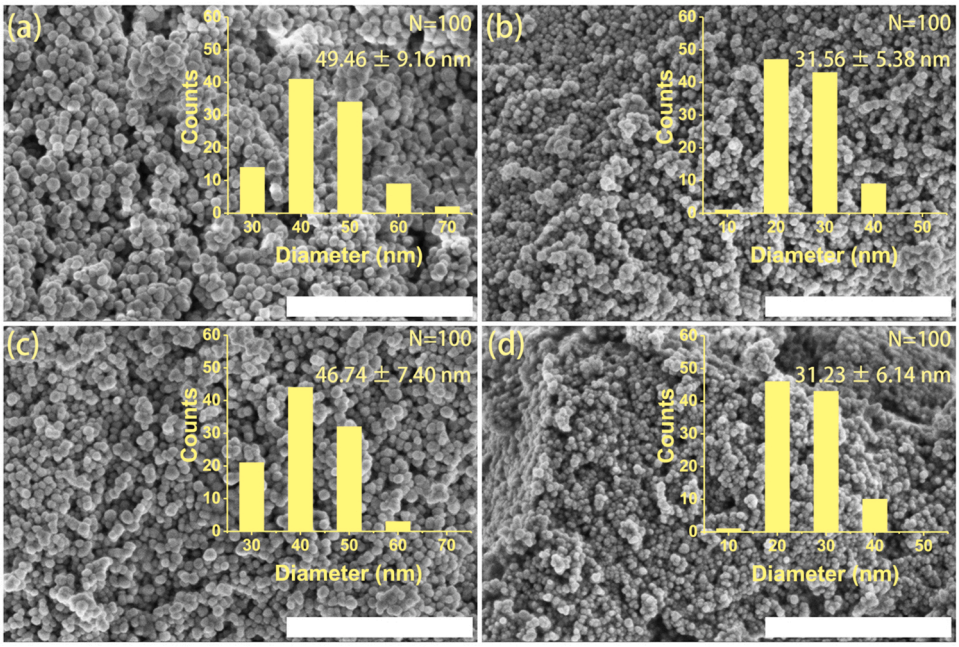

Fig. 3. The SEM images of (a) 60-MI-ZGO-750-EDTA, (b) 60-NI-ZGO-750-EDTA, (c) 80-MI-ZGO-750-EDTA and (d) 80-NI-ZGO-750-EDTA (all bars are 1 μm). Inset are the statistical size of randomly selected 100 nanoparticles.

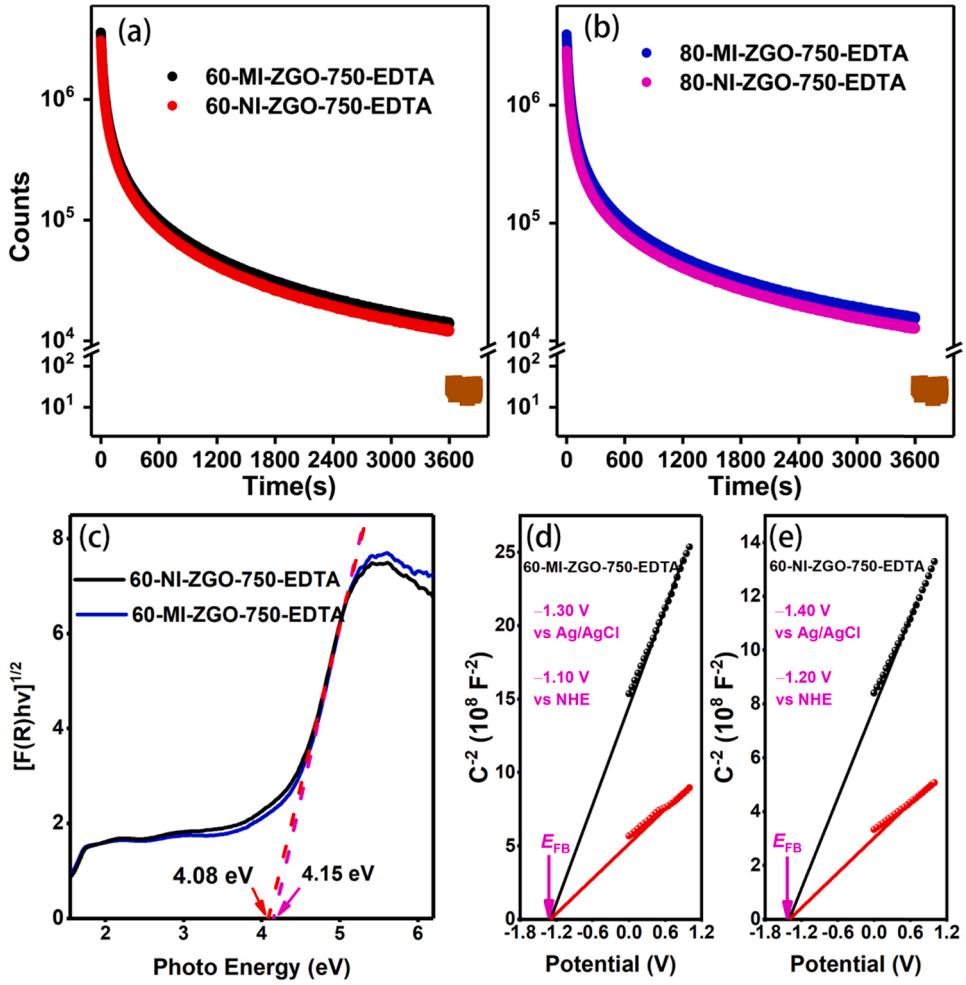

Fig. 4. Afterglow decay curves of (a) 60-MI/NI-ZGO-750-EDTA and (b) 80-MI/NI-ZGO-750-EDTA (brown lines represent background). 100 mg solid samples were measured with EM slit of 20 nm, immediately after the stoppage of 254 nm UV lamp (6 W) for 5 min lighting. (c) Kubelka-Munk plots of 60-MI/NI-ZGO-750-EDTA measured by DRS spectra. (d-e) Mott-Schottky curve of (d) 60-MI-ZGO-750-EDTA and (e) 60-NI-ZGO-750-EDTA.

semiconductors of 60-MI/NI-ZGO-750-EDTA. E_{CB} is around to the flat band potential (E_{FB}), thus E_{CB} and E_{VB} of 60-MI-ZGO-750-EDTA are about − 1.10 eV and 3.05 eV (NHE), and those of 60-NI-ZGO-750-EDTA are about − 1.20 eV, and 2.88 eV (NHE). Accordingly, for 60-MI/NI-ZGO-750-EDTA, the position of E_{CB} is more negative than E(O_2/$^{\bullet}O_2^-$) (−0.28 eV, NHE), and the position of E_{VB} is more positive than E($^{\bullet}$OH/H_2O) (2.27 eV, NHE), illustrating the capability of 60-MI/NI-ZGO-750-EDTA to continuously generate •OH from H_2O with photo-holes, and $\bullet O_2^-$ from O_2 with photo-electrons. Certainly, the photo-holes are also active species for catalytic degradation, which has been systematically proved by the experiments of trapping holes, •OH, and $\bullet O_2^-$ by different scavengers in our previous research [37].

3.3. Selective adsorption and day-and-night degradation of TC by MI/NI-ZGO-750-EDTA

TC adsorption and around-the-clock degradation are examined by C/C_0, wherein C and C_0 are the real-time concentration and initial concentration of TC. The experimental set-up is all follows: the catalysts are first settled in the dark for 12 h to release the remaining afterglow, so the first 1 h stirring in the dark after addition of TC solution into the dispersions of catalysts can be regarded as the adsorption of TC onto catalyst, and then illuminating the mixtures of TC and catalyst-dispersions for 2 h by a 500 W Xe lamp (with a 420 nm filter) is simulation of in situ visible-light-lighting degradation (day time), finally the followed stirring in-the-dark for 4 h is imitation of the degradation at night time.

We first searched the best concentration of catalyst, and 60/80-MI-ZGO-750-EDTA at 0.25, 0.50, 0.75 and 1.25 g·L^{-1} were examined for the adsorption and around-the-clock degradation of 25 mg·L^{-1} TC (Fig. 5a,b, Fig. S6a and Tab. S1). The 1-h adsorption of TC onto the catalysts is almost independent of the concentration of the catalysts, but the in situ visible-light lighting and in-the-dark degradation are gradually improved with the increasing of catalysts concentration. When increased to more than 0.75 g·L^{-1}, the in situ-lighting and in-the-dark degradation are almost saturated (the stable C/C_0 of nearly 1 in Fig. 5d proves the pure TC solution is stable upon the irradiation for 2 h by above-mentioned visible-light). Therefore, the best catalyst concentration is set at 0.75 g·L^{-1}.

To examine the imprinting effect of the synthesized catalysts, we compared TC adsorption and degradation by 0.75 g·L^{-1} of 60/80-MI-ZGO-750-EDTA and 60/80-NI-ZGO-750-EDTA (Fig. 5c, Fig. S6b and Tab. S2). The 60/80-NI-ZGO-750-EDTA also have adsorption and degradation towards TC, but with lower percentages than the corresponding 60/80-MI-ZGO-750-EDTA. The imprinting factor (IF), defined as the adsorption or degradation percent ratio of MI- and NI- ZGO-750-EDTA, are in the range of 1.3–2.2, demonstrating the fine imprinting effect. The 60-MI-ZGO-750-EDTA exhibits higher IF under in situ-lighting, while 80-MI-ZGO-750-EDTA has higher IF in-the-dark. It is worthy to note that the degradation percent in the dark of 80-MI-ZGO-

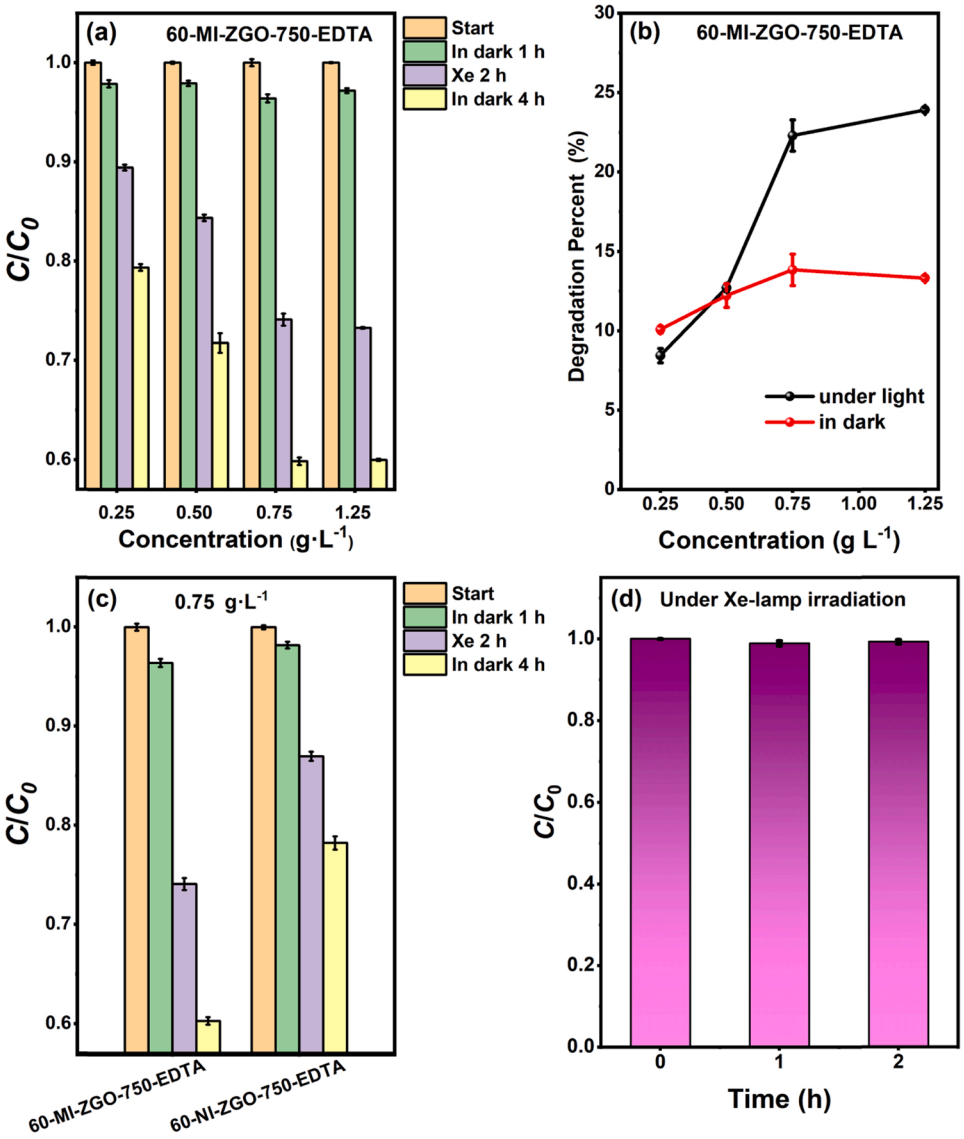

Fig. 5. Adsorption and degradation of TC by 60-MI/NI-ZGO-750-EDTA under in situ lighting and then in the dark: (a) adsorption and degradation of TC; and (b) degradation percent of TC by 60-MI-ZGO-750-EDTA at different concentration (0.25, 0.50, 0.75 and 1.25 g·L^{-1}); (c) TC degradation by 0.75 g·L^{-1} of 60-MI-ZGO-750-EDTA and 60-NI-ZGO-750-EDTA; (d) stability of pure TC solution irradiated by 500 W Xe lamp with 420 nm filter for 2 h. C and C_0 are the real-time concentration and initial concentration of TC (c. a. 25 mg·L^{-1}).

750-EDTA is 80% of its degradation percent under in situ-lighting, demonstrating the high potential as the day-and-night catalyst. As the degradation percent of TC of 60-MI-ZGO-750-EDTA is higher than that of 80-MI-ZGO-750-EDTA, thus in the subsequent study, the 60-MI/NI-ZGO-750-EDTA at 0.75 g·L^{-1} is used as the catalyst.

To evaluate the selectivity, OTC, one of the structure analogues are used as target. The adsorption and day-and-night degrading towards TC and OTC in pure or mixed solutions by 0.75 g·L^{-1} of 60-MI/NI-ZGO-750-EDTA are demonstrated by Fig. 5c, Fig. S7 and Table 1. For pure solutions, the IFs of TC are 2.2–4.1 times of OTC, while for the mixed solutions, the IFs of TC are 1.6–1.9 times of OTC, demonstrating the good selectivity of TC over OTC for adsorption and day-and-night degradation.

3.4. Anti-interference of TC afterglow-catalytic degradation by 60-MI-ZGO-750-EDTA

Besides OTC, we chose MG with deep color, high absorption of visible light and efficient degradation by ZGO-750-EDTA [37], as the typical interference of the environmental coexistence to evaluate the selectivity and anti-interference of TC afterglow-catalytic degradation. For afterglow-catalytic degradation, only the catalyst was lighted (for 2 h by a 500 W Xe lamp with 420 nm filter), and then TC, OTC, MG, or mixture of TC/OTC, TC/MG (25 mg·L^{-1} of TC and OTC, 50 mg·L^{-1} of MG) were added into the lighted dispersions of

Table 1
Adsorption and day-and-night degradation percent of TC and OTC in pure or mixed solutions by 0.75 g·L^{-1} of 60-MI/NI-ZGO-750-EDTA and corresponding IF.

Mode		Target	Percent (%)		IF
			60-MI-ZGO-750-EDTA	60-NI-ZGO-750-EDTA	
Pure	Adsorption	TC	3.59 ± 0.41	1.80 ± 0.34	1.99
		OTC	5.17 ± 1.48	10.66 ± 1.22	0.49
	Day-degradation	TC	22.29 ± 0.98	11.72 ± 0.79	1.90
		OTC	10.19 ± 0.73	18.40 ± 0.54	0.55
	Night-degradation	TC	14.27 ± 0.98	8.73 ± 0.63	1.63
		OTC	3.45 ± 0.27	4.75 ± 0.59	0.73
Mixed	Adsorption	TC	3.92 ± 1.97	2.88 ± 0.58	1.36
		OTC	4.08 ± 2.02	5.79 ± 0.59	0.70
	Day-degradation	TC	8.61 ± 3.17	7.31 ± 1.36	1.18
		OTC	8.12 ± 3.15	11.03 ± 2.19	0.74
	Night-degradation	TC	7.67 ± 3.08	4.98 ± 2.77	1.54
		OTC	7.83 ± 1.09	8.34 ± 2.23	0.94

60-MI/NI-ZGO-750-EDTA (0.75 g·L^{-1}), and then the mixtures were stirred in the dark for 4 h.

Fig. 6 and Table 2 compare the afterglow-catalytic degradation of TC, OTC and MG in pure solutions. The afterglow-degradation percent by 60-MI-ZGO-750-EDTA /60-NI-ZGO-750-EDTA are 11.62%/5.56% for TC, 10.55%/14.99% for OTC and 18.51%/30.92% for MG respectively, giving the IF of 2.09 for TC, 0.70 for OTC and 0.60 for MG. The much higher percent of the afterglow-degrading of OTC and MG by 60-NI-ZGO-750-EDTA illustrates OTC and MG are much more easily degraded, especially MG, which has been proved in our previous work [37]. However, the imprinting of TC into ZGO significantly lowers the afterglow-degrading capability towards OTC and MG, but increase the afterglow-degrading power of TC, demonstrating the great potential of 60-MI-ZGO-750-EDTA to degrade the low concentration of TC even in the presence of the interference with high concentration.

Fig. 7 and Table 2 show the afterglow-degrading of TC/OTC and TC/MG in the mixed solutions. Compared with the degradation of TC, OTC or MG in pure solutions (Fig. 6), the degradation percent is lowered in the mixed solutions, which makes sense as the carriers are shared to degrade TC/OTC and TC/MG. However, the difference between the degradation of TC by 60-MI-ZGO-750-EDTA / 60-NI-ZGO-750-EDTA is both enlarged, 10.32% / 3.59% in TC/OTC mixture with IF of 2.87, and 8.61% / 1.89% in TC/MG mixture with IF of 4.56. In contrast, the degradation of OTC and MG by 60-MI-ZGO-750-EDTA / 60-NI-ZGO-750-EDTA is 10.81% / 13.39% in TC/OTC mixture with IF of 0.81, and 19.55% / 22.30% in TC/MG mixture with IF of 0.88 respectively. In pure solutions, the IF of TC is 3 times of OTC, while in mixed solutions, the IF of TC is 3.5 times of OTC, demonstrating the great potential for selective TC degradation in the presence of structure analogues. It is worth highlighting that the concentration of MG used is 2 times of TC, and MG is easier to be degraded [37], thus 60-NI-ZGO-750-EDTA show higher degradation percent towards MG in both the pure and mixed solutions, but 60-MI-ZGO-750-EDTA displays much higher selectivity in degrading TC. Take the MG degradation by 60-NI-ZGO-750-EDTA as the reference, the degrading power to TC of 60-MI-ZGO-750-EDTA is elevated to 3.5 (2.09/0.60) times in pure solutions and 5.2 (4.56/0.88) times in mixed solutions.

Table 2
Selectivity of afterglow-catalytic degradation of TC, OTC and MG by 60-MI/NI-ZGO-750-EDTA in pure or mixed solutions.

Mode	Target	Degrading percent (%)		IF
		60-MI-ZGO-750-EDTA	60-NI-ZGO-750-EDTA	
Pure solution	TC	11.62 ± 0.58	5.56 ± 1.24	2.09
	OTC	10.55 ± 0.34	14.99 ± 0.35	0.70
	MG	18.51 ± 2.68	30.92 ± 1.40	0.60
Mixed TC/OTC	TC	10.32 ± 0.77	3.59 ± 0.88	2.87
	OTC	10.81 ± 1.23	13.39 ± 0.74	0.81
Mixed TC/MG	TC	8.61 ± 0.57	1.89 ± 0.68	4.56
	MG	19.55 ± 1.53	22.30 ± 0.66	0.88

The merit of afterglow-catalysis over traditional photo-catalysis lies in three aspects, that is, afterglow-catalysis can proceed after the cease of external lighting, avoid the light-scattering of catalysts and thus enable the usage of large dose of catalyst and degradation at deep depth, and enhance the selectivity of degradation. The first two advantages are well-documented, while the latter is proved by comparing the afterglow- and photo- catalytic degradation of TC in the mixtures of TC/OTC and TC/MG (Fig. 7 vs Fig. S8). The superfine selectivity of afterglow-catalysis has been elucidated as above-mentioned, however, for the photo-catalytic degradation (lighted by Xe lamp with 420 nm filter for 4 h) in the mixture of TC/OTC and TC/MG, 60-MI-ZGO-750-EDTA and 60-NI-ZGO-750-EDTA nearly have the same degradation percent towards TC (Fig. S8 and Tab. S3). Although the degradation percent of OTC or MG by 60-MI-ZGO-750-EDTA is lower than that of 60-NI-ZGO-750-EDTA, the overall selectivity is much poorer than those of afterglow-catalysis. Take the MG degradation by 60-NI-ZGO-750-EDTA as the reference, the photo-catalytic degrading power to TC of 60-MI-ZGO-750-EDTA is only elevated to 1.5 (0.96/0.66) times in mixed solutions, in contrast, the afterglow-catalytic degrading power of TC is

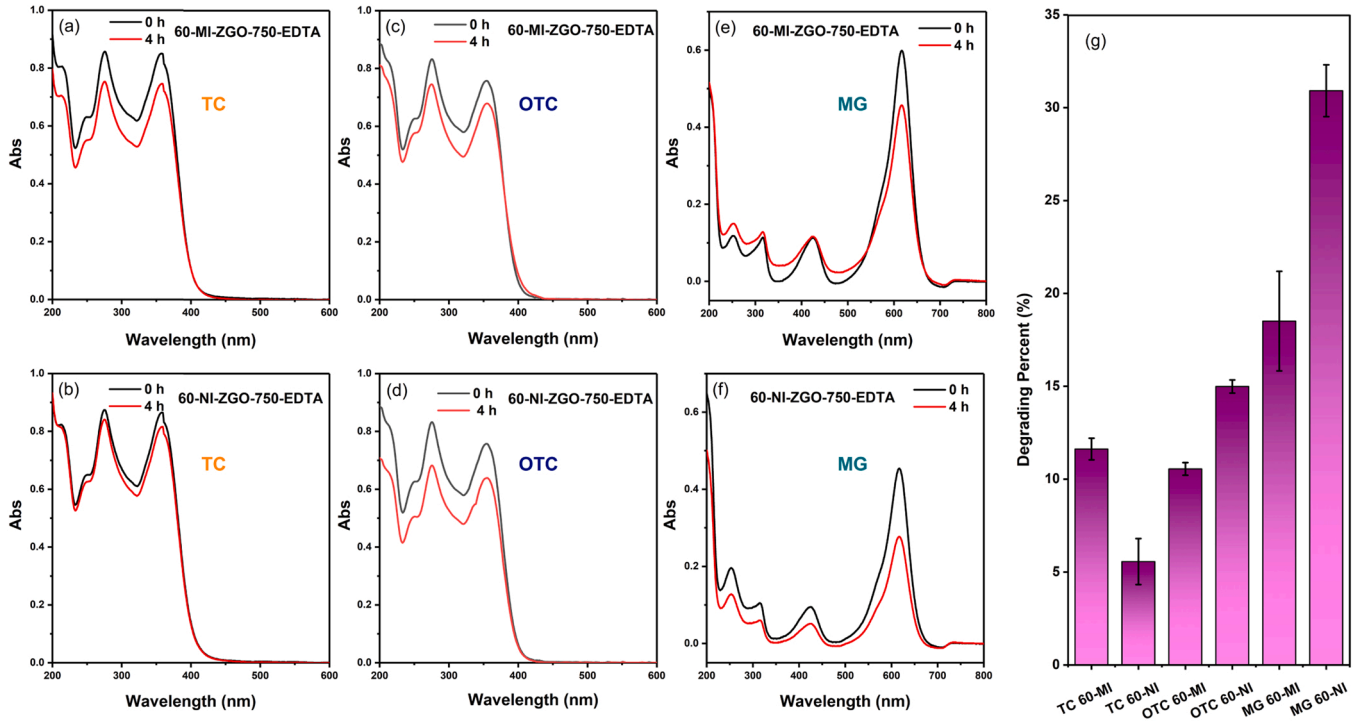

Fig. 6. Afterglow-catalytic degradation of TC, OTC, and MG in pure solutions by 60-MI/NI-ZGO-750-EDTA (0.75 g L^{-1}). The UV-Vis spectra of the supernatant from (a, b) TC, (c, d) OTC and (e, f) MG degradation at 0 and 4 h; and (g) the corresponding degradation percent of TC, OTC and MG. The initial concentration of TC and OTC is 25 mg L^{-1}, and that of MG is 50 mg L^{-1}.

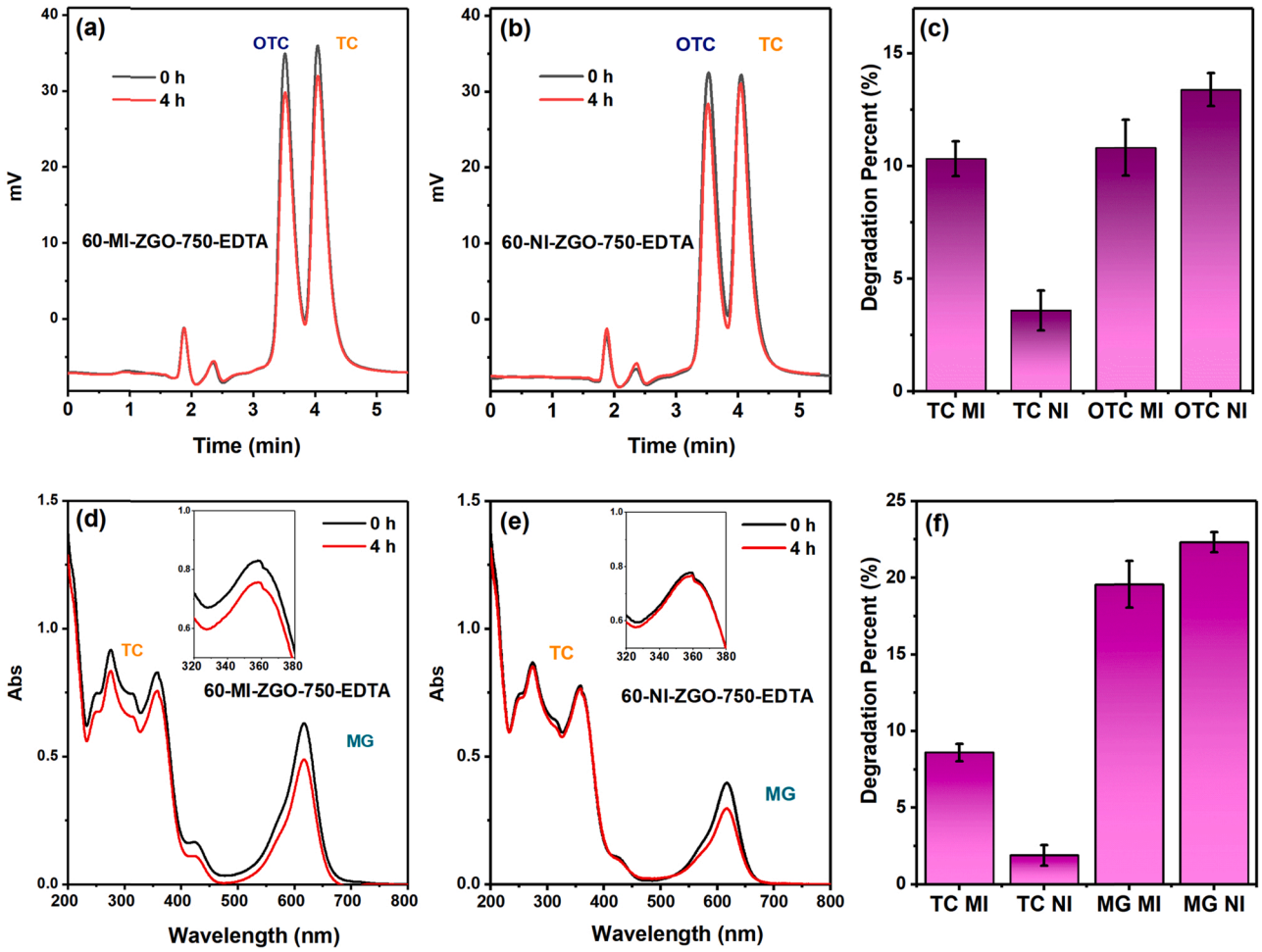

Fig. 7. Afterglow-catalytic degradation of (a-c) TC/OTC and (d-f) TC/MG in the mixed solutions by 60-MI/NI-ZGO-750-EDTA. (a-c) HPLC chromatograms of the supernatant from degrading TC/OTC by (a) 60-MI-ZGO-750-EDTA and (b) 60-NI-ZGO-750-EDTA at 0 and 4 h; and (c) the corresponding degradation percent of TC and OTC; (d-f) UV-Vis spectra of the supernatant from degrading TC/MG by (d) 60-MI-ZGO-750-EDTA and (e) 60-NI-ZGO-750-EDTA at 0 and 4 h; and (f) the corresponding degradation percent of TC and MG. The initial concentration of TC and OTC is 25 mg L^{-1}, and that of MG is 50 mg L^{-1}.

elevated to 5.2 times as above-mentioned.

As demonstrated in Fig. 4, both MI- and NI-ZGO-750-EDTA have similar afterglow property, and meet the energy requirements of generating •OH from H_2O, and $•O_2^-$ from dissolved O_2 with photo-generated carriers. The active species responsible for degradation are the same as our previous work [37], including holes, •OH, and $•O_2^-$. The main difference between MI- and NI-ZGO-750-EDTA is the specific binding sites of TC in MI-ZGO-750-EDTA, which is proved by the adsorption isomers in Fig. S9 (SI). In afterglow-catalysis, degradation of the targets happens after stoppage of lighting the catalysts, just in virtue of the gradually released holes and electrons trapped in the traps to generate those active species, thus in a slow speed. Then TC molecules around MI-ZGO-750-EDTA surface have sufficient time to migrate into the selective sites, being adsorbed and then degraded successively, which is proved by the continuous degradation with extension of time (Fig. S10 in SI). In photo-catalysis and day-and-night modes, however, TC, OTC and MG are also lighted with catalysts for 4 and 2 h, and thus degraded rapidly by large amount of those active species, with higher degradation percent but lower selectivity. The longer lighting time of the targets and catalysts, the higher degradation percent but the lower selectivity.

The prepared 60-MI/NI-ZGO-750-EDTA exhibits fine recyclability, as the three usages show nearly the identic degradation efficiency and IF (Fig. S11). Cr^{3+} might have influence of environmental safety [49], but in MI/NI-ZGO-750-EDTA, Cr^{3+} has been doped into the lattice of ZGO via calcination and is very tiny [46], and exudation of Cr^{3+} during usage is not detected by inductively couple plasma-atomic emission spectrometry (less than 0.004 mg·L^{-1}).

3.5. PL self-report of real-time concentration of TC during degradation

As the luminescence center of ZGO, Cr^{3+}can emit characteristic PL at 698 nm when the photo-generated holes and electrons recombine at Cr^{3+}. In the presence of TC, the separated photo-generated holes and electrons can also react with the H_2O and O_2 adsorbed on the surface of ZGO to generate $^•OH$ and $^•O_2^-$, and then, $^•OH$ and $^•O_2^-$ interact with TC and results in the degradation of TC (Scheme 1). Based on the competitive relationship between the separation and recombination of photo-generated carriers, we find that there is a corresponding relationship between the PL emission of ZGO at 698 nm and the concentration of TC. At the beginning, the concentration of TC is high, the separated photo-carriers are mainly used to generate the reactive oxygen species ($^•OH$ and $^•O_2^-$), the characteristic PL intensity of Cr^{3+} at 698 nm is quenched. With TC degradation goes on, the concentration of TC gradually decreases, more photo-carriers are recombined to emit PL, so that the intensity gradually recovers. Therefore, the PL intensity at 698 nm of the mixed dispersion of the 60-MI-ZGO-750-EDTA and TC can accurately reflect the real-time concentration of TC during degradation.

We constructed the standard curve between TC concentration and PL intensity of 60-MI-ZGO-750-EDTA dispersions (0.75 g·L^{-1}). As shown in

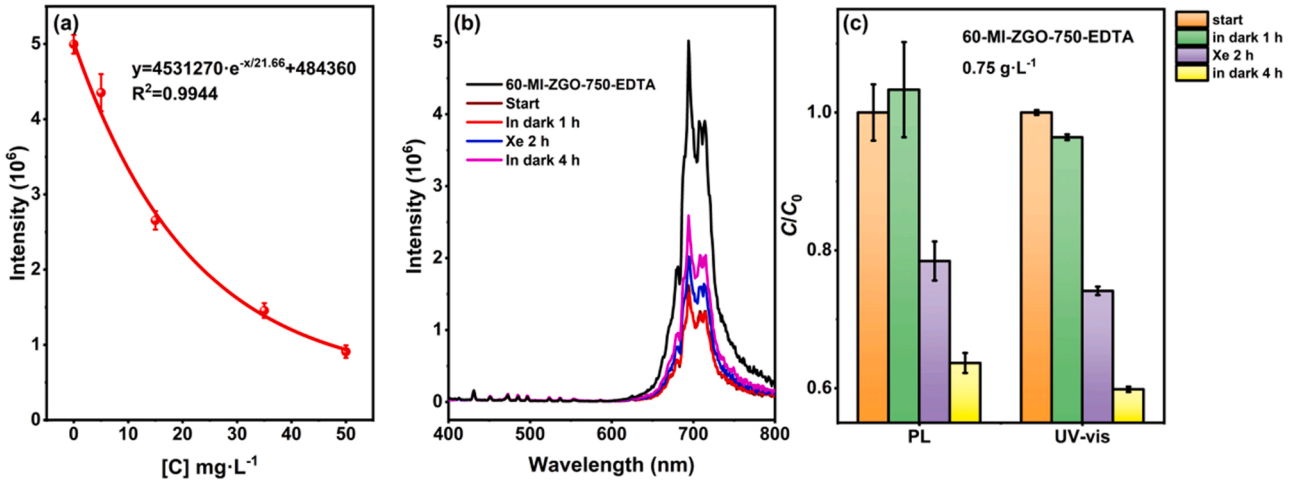

Fig. 8. PL self-reporting TC concentration by 60-MI-ZGO-750-EDTA during TC degradation. (a) standard curve between PL intensity at 698 nm of 0.75 g·L^{-1} 60-MI-ZGO-750-EDTA dispersion and TC concentration; (b) emission spectra of dispersions of 60-MI-ZGO-750-EDTA and TC at different intervals; and (c) degradation of TC measured by PL self-reporting and UV–vis absorption spectra, where C_0 and C are the initial and real-time concentration of TC respectively.

Fig. 8a, the standard curve shows an exponential relationship ($y = 4531270 \cdot e^{-x/21.66} + 484360$, $R^2 = 0.9944$, y stands for the PL intensity and x stands for TC concentration). After that, we use 0.75 g·L^{-1} 60-MI-ZGO-750-EDTA to degrade TC (25 mg·L^{-1}), and measure the PL emission spectra of the dispersions at different interval. We determine the real-time concentration of TC relying on the standard curve, and compare the result of PL self-report and UV-vis absorption spectra.

Fig. 8b exhibits the emission spectra of the dispersions taken out at different intervals. The PL intensity at 698 nm is maximally quenched (Fig. 8b, wine red line) when TC is added, and after adsorption in the dark for 1 h, the PL intensity has little change (Fig. 8b, red line). After the in situ-lighting by Xe lamp (with 420 nm filter) for 2 h, the PL intensity recovers partly (Fig. 8b, blue line), and after the followed stirring in the dark for 4 h, the PL intensity continues to restore (Fig. 8b, pink line), indicating the TC concentration is gradually decreased. The results of PL self-reporting and UV–vis absorption are shown in Fig. 8c. For 2 h in situ irradiation, PL self-reporting reveals TC degradation percent of (24.86 ± 2.84)%, and UV–vis absorption displays TC degradation percent of (22.23 ± 0.61)%. For 4 h degradation in the dark, TC degradation percent reported by PL self-reporting and UV–vis absorption is (14.79 ± 1.45)% and (14.27% ± 0.38)% respectively. These data illustrate that whether in situ-lighting or in-the-dark, the degradation percent measured by PL self-reporting and UV–vis absorption is consistent within the error range, confirming the feasibility of PL self-reporting and the complete degradation [37] of TC by 60-MI-ZGO-750-EDTA.

4. Conclusion

Combining molecular imprinting with afterglow-catalysis, we construct a novel design for the round-the-clock catalyst to selectively degrade the imprinted template. The TC imprinted MI-ZGO-750-EDTA is used as the example. The highest degradation in-the-dark (night time) is 80% of in situ lighting (day time). The selectivity in both the photo-and afterglow-catalytic mode is fine, but the afterglow-catalysis has higher selectivity. For afterglow-catalytic degradation, the IF for TC is 3 times of OTC and 3.5 times of MG in pure solutions, while in mixed solutions, IF for TC is 3.5 times of OTC and 5.2 times of MG. Besides, the smart MI-ZGO-750-EDTA can simply self-report the real-time degradation process, just by measuring the PL intensity of MI-ZGO-750-EDTA. This work reports the first example of the smart catalysts capable of selectively degrading the target day-and-night and self-reporting the degradation process, thus would catch wide interest among the fields of catalysis, environment protection, chemical engineering and functional materials.

CRediT authorship contribution statement

Ye Zhang and Zheng-Wu Wang: Conceptualization, Methodology, Investigation, Data curation, Formal analysis, Writing – original draft preparation, Visualization. **He-Fang Wang:** Conceptualization, Methodology, Supervision, Writing – reviewing and editing, Visualization, Resources, Funding acquisition. **Yi-Zhou Zhu:** Conceptualization, Methodology, Writing – reviewing and editing, Visualization, Resources. **Xiao-Ting Yang:** Data curation.

Declaration of Competing Interest

The authors declare that they have no known competing financial interests or personal relationships that could have appeared to influence the work reported in this paper.

Acknowledgments

The authors appreciate the support by the National Natural Science Foundation of China (No. 21974072 and 21575070), and the Fundamental Research Funds for the Central Universities (China).

Appendix A. Supporting information

Supplementary data associated with this article can be found in the online version at doi:10.1016/j.apcatb.2021.121025.

References

[1] Z. Zhu, X. Tang, S. Kang, P. Huo, M. Song, W. Shi, Z. Lu, Y. Yan, Constructing of the magnetic photocatalytic nanoreactor MS@FCN for cascade catalytic degrading of tetracycline, J. Phys. Chem. C. 120 (2016) 27250–27258.
[2] K.H. Chu, Y.A.J. Al-Hamadani, C.M. Park, G. Lee, M. Jang, A. Jang, N. Her, A. Son, Y. Yoon, Ultrasonic treatment of endocrine disrupting compounds, pharmaceuticals, and personal care products in water: a review, Chem. Eng. J. 327 (2017) 629–647.
[3] G. Liu, K. Han, H. Ye, C. Zhu, Y. Gao, Y. Liu, Y. Zhou, Graphene oxide/triethanolamine modified titanate nanowires as photocatalytic membrane for water treatment, Chem. Eng. J. 320 (2017) 74–80.
[4] C. Santhosh, V. Velmurugan, G. Jacob, S.K. Jeong, A.N. Grace, A. Bhatnagar, Role of nanomaterials in water treatment applications: a review, Chem. Eng. J. 306 (2016) 1116–1137.
[5] Y. Guo, L. Yan, X. Li, T. Yan, W. Song, T. Hou, C. Tong, J. Mu, M. Xu, Goethite/biochar-activated peroxymonosulfate enhances tetracycline degradation: inherent roles of radical and non-radical processes, Sci. Total Environ. 783 (2021), 147102.
[6] H.R. Sun, F. Guo, J.J. Pan, W. Huang, K. Wang, W.L. Shi, One-pot thermal polymerization route to prepare N-deficient modified g-C3N4 for the degradation

of tetracycline by the synergistic effect of photocatalysis and persulfate-based advanced oxidation process, Chem. Eng. J. 406 (2021), 126844.
[7] J.L. Wang, R. Zhuan, Degradation of antibiotics by advanced oxidation processes: an overview, Sci. Total Environ. 701 (2020), 135023.
[8] K. Wang, T. Zhuang, Z. Su, M. Chi, H. Wang, Antibiotic residues in wastewaters from sewage treatment plants and pharmaceutical industries: occurrence, removal and environmental impacts, Sci. Total Environ. 788 (2021), 147811.
[9] A.S. Oberoi, Y.Y. Jia, H.Q. Zhang, S.K. Khanal, H. Lu, Insights into the fate and removal of antibiotics in engineered biological treatment systems: a critical review, Environ. Sci. Technol. 53 (2019) 7234–7264.
[10] N.H. Tran, H.J. Chen, M. Reinhard, F. Mao, K.Y.H. Gin, Occurrence and removal of multiple classes of antibiotics and antimicrobial agents in biological wastewater treatment processes, Water Res. 104 (2016) 461–472.
[11] J. Guo, L. Wang, X. Wei, Z.A. Alothman, M.D. Albaqami, V. Malgras, Y. Yamauchi, Y. Kang, M. Wang, W. Guan, X. Xu, Direct Z-scheme CuInS2/Bi2MoO6 heterostructure for enhanced photocatalytic degradation of tetracycline under visible light, J. Hazard. Mater. 415 (2021), 125591.
[12] T. Tang, Z. Yin, J. Chen, S. Zhang, W. Sheng, W. Wei, Y. Xiao, Q. Shi, S. Cao, Novel p-n heterojunction Bi2O3/Ti3+-TiO2 photocatalyst enables the complete removal of tetracyclines under visible light, Chem. Eng. J. 417 (2021), 128058.
[13] X.L. Song, Y. Wang, T. Zhu, J.L. Liu, S.W. Zhang, Facile synthesis a novel core-shell amino functionalized MIL-125(Ti) micro-photocatalyst for enhanced degradation of tetracycline hydrochloride under visible light, Chem. Eng. J. 416 (2021), 129126.
[14] Y.X. Wu, X.S. Zhao, S.B. Huang, Y.H. Li, X.Q. Zhang, G.C. Zeng, L.S. Niu, Y. Ling, Y. Q. Zhang, Facile construction of 2D g-C3N4 supported nanoflower-like NaBiO3 with direct Z-scheme heterojunctions and insight into its photocatalytic degradation of tetracycline, J. Hazard. Mater. 414 (2021), 125547.
[15] X. Hou, Z.Q. Wang, J.J. Chen, J.C. Wang, Q.S. Lu, D. Wu, Facile construction of silver-based solid solution heterophase for efficient visible-light-driven photocatalytic degradation of tetracycline, Chem. Eng. J. 414 (2021), 128915.
[16] A. Serra, E. Gomez, J. Michler, L. Philippe, Facile cost-effective fabrication of Cu@Cu2O@CuO-microalgae photocatalyst with enhanced visible light degradation of tetracycline, Chem. Eng. J. 413 (2021), 127477.
[17] K. Wang, J. Li, G. Zhang, Ag-bridged Z-Scheme 2D/2D Bi5FeTi3O15/g-C3N4 heterojunction for enhanced photocatalysis: mediator-induced interfacial charge transfer and mechanism insights, ACS Appl. Mater. Interfaces 11 (2019) 27686–27696.
[18] F. Rong, Q. Lu, H. Mai, D. Chen, R.A. Caruso, Hierarchically porous WO3/CdWO4 fiber-in-tube nanostructures featuring readily accessible active sites and enhanced photocatalytic effectiveness for antibiotic degradation in water, ACS Appl. Mater. Interfaces 13 (2021) 21138–21148.
[19] Y. Paz, Preferential photodegradation - why and how? C. R. Chim. 9 (2006) 774–787.
[20] X. Shen, L. Zhu, H. Yu, H. Tang, S. Liu, W. Li, Selective photocatalysis on molecular imprinted TiO_2 thin films prepared via an improved liquid phase deposition method, N. J. Chem. 33 (2009) 1673–1679.
[21] G. Zhang, W. Choi, S.H. Kim, S.B. Hong, Selective photocatalytic degradation of aquatic pollutants by titania encapsulated into FAU-type zeolites, J. Hazard. Mater. 188 (2011) 198–205.
[22] L. Li, X. Zheng, Y. Chi, Y. Wang, X. Sun, Q. Yue, B. Gao, S. Xu, Molecularly imprinted carbon nanosheets supported TiO_2: Strong selectivity and synergic adsorption-photocatalysis for antibiotics removal, J. Hazard. Mater. 383 (2020), 121211.
[23] C.C. de Escobar, M.A. Lansarin, J.H.Z. dos Santos, Synthesis of molecularly imprinted photocatalysts containing low TiO_2 loading: evaluation for the degradation of pharmaceuticals, J. Hazard. Mater. 306 (2016) 359–366.
[24] Z.Y. Lu, F. Chen, M. He, M.S. Song, Z.F. Ma, W.D. Shi, Y.S. Yan, J.Z. Lan, F. Li, P. Xiao, Microwave synthesis of a novel magnetic imprinted TiO_2 photocatalyst with excellent transparency for selective photodegradation of enrofloxacin hydrochloride residues solution, Chem. Eng. J. 249 (2014) 15–26.
[25] Z. Wang, T. Qiu, L. Guo, J. Ye, L. He, X. Li, The building of molecularly imprinted single hole hollow particles: a miniemulsion polymerization approach, Chem. Eng. J. 357 (2019) 348–357.
[26] B. Tang, H. Shi, Z. Fan, G. Zhao, Preferential electrocatalytic degradation of 2,4-dichlorophenoxyacetic acid on molecular imprinted mesoporous SnO_2 surface, Chem. Eng. J. 334 (2018) 882–890.
[27] Y. Cheng, T. Chen, D. Fu, J. Liu, A molecularly imprinted nanoreactor based on biomimetic mineralization of bi-enzymes for specific detection of urea and its analogues, Sens. Actuators B-Chem. 350 (2022), 130909.
[28] T. Chen, A. Zhang, Y. Cheng, Y. Zhang, D. Fu, M. Liu, A. Li, J. Liu, A molecularly imprinted nanoreactor with spatially confined effect fabricated with nano-caged cascaded enzymatic system for specific detection of monosaccharides, Biosens. Bioelectron. 188 (2021), 113355.
[29] M. Yoshikawa, K. Tharpa, S.-O. Dima, Molecularly imprinted membranes: past, present, and future, Chem. Rev. 116 (2016) 11500–11528.
[30] X. Zhou, C. Lai, D. Huang, G. Zeng, L. Chen, L. Qin, P. Xu, M. Cheng, C. Huang, C. Zhang, C. Zhou, Preparation of water-compatible molecularly imprinted thiol-functionalized activated titanium dioxide: selective adsorption and efficient photodegradation of 2, 4-dinitrophenol in aqueous solution, J. Hazard. Mater. 346 (2018) 113–123.
[31] Q. Yuan, D. Zhang, P. Yu, R. Sun, H. Javed, G. Wu, P.J.J. Alvarez, Selective adsorption and photocatalytic degradation of extracellular antibiotic resistance genes by molecularly-imprinted graphitic carbon nitride, Environ. Sci. Technol. 54 (2020) 4621–4630.
[32] R. Fiorenza, A. Di Mauro, M. Cantarella, C. Iaria, E.M. Scalisi, M.V. Brundo, A. Gulino, L. Spitaleri, G. Nicotra, S. Dattilo, S.C. Carroccio, V. Privitera, G. Impellizzeri, Preferential removal of pesticides from water by molecular imprinting on TiO_2 photocatalysts, Chem. Eng. J. 379 (2020), 122309.
[33] J. Zhang, B. Tang, G. Zhao, Selective photoelectrocatalytic removal of dimethyl phthalate on high-quality expressed molecular imprints decorated specific facet of single crystalline TiO_2 photoanode, Appl. Catal. B-Environ. 279 (2020), 119364.
[34] B. Tang, J. Zhang, N. Yang, G. Zhao, Selective photoelectrocatalytic removal of environmental pollutants on molecular imprints decorated TiO_2 single crystalline nanoarrays, Chem. Eng. J. 383 (2020), 123188.
[35] M. Cantarella, A. Di Mauro, A. Gulino, L. Spitaleri, G. Nicotra, V. Privitera, G. Impellizzeri, Selective photodegradation of paracetamol by molecularly imprinted ZnO nanonuts, Appl. Catal. B-Environ. 238 (2018) 509–517.
[36] D. Sharma, M. Ashaduzzaman, M. Golabi, A. Shriwastav, K. Bisetty, A. Tiwari, Studies on bacterial proteins corona interaction with saponin imprinted Zno nanohoneycombs and their toxic responses, ACS Appl. Mater. Interfaces 7 (2015) 23848–23856.
[37] Y. Zhang, Z.-W. Wang, X. Ji, T. Wang, X.-T. Yang, H.-F. Wang, Afterglow-catalysis and self-reporting of pollutant degradation by ethylenediaminetetraacetic acid disodium-etched Cr:ZnGa2O4, J. Phys. Chem. C. 125 (2021) 9096–9106.
[38] J. Zhou, J. Huang, Y. Xia, H. Ou, Z. Li, Two-in-one ultraviolet persistent luminescent catalyst suitable for high concentration photodegradation, Sci. Total Environ. 699 (2020), 134342.
[39] A. Bessiere, S.K. Sharma, N. Basavaraju, K.R. Priolkar, L. Binet, B. Viana, A.J.J. Bos, T. Maldiney, C. Richard, D. Scherman, D. Gourier, Storage of visible light for long-lasting phosphorescence in chromium-doped zinc gallate, Chem. Mater. 26 (2014) 1365–1373.
[40] T. Maldiney, A. Bessiere, J. Seguin, E. Teston, S.K. Sharma, B. Viana, A.J.J. Bos, P. Dorenbos, M. Bessodes, D. Gourier, D. Scherman, C. Richard, The in vivo activation of persistent nanophosphors for optical imaging of vascularization, tumours and grafted cells, Nat. Mater. 13 (2014) 418–426.
[41] Z. Li, Y. Zhang, X. Wu, L. Huang, D. Li, W. Fan, G. Han, Direct aqueous-phase synthesis of sub-10 nm "luminous pearls" with enhanced in vivo renewable near-infrared persistent luminescence, J. Am. Chem. Soc. 137 (2015) 5304–5307.
[42] Z. Zhou, W. Zheng, J. Kong, Y. Liu, P. Huang, S. Zhou, Z. Chen, J. Shi, X. Chen, Rechargeable and LED-activated $ZnGa_2O_4$:Cr^{3+} near-infrared persistent luminescence nanoprobes for background-free biodetection, Nanoscale 9 (2017) 6846–6853.
[43] J. Bai, J. Sun, X. Zhu, J. Liu, H. Zhang, X.-B. Yin, L. Liu, Enhancement of solar-driven photocatalytic activity of BiOI nanosheets through predominant exposed high energy facets and vacancy engineering, Small 16 (2020), 1904783.
[44] F. Guo, X.L. Huang, Z.H. Chen, H.J. Ren, M.Y. Li, L.Z. Chen, MoS_2 nanosheets anchored on porous $ZnSnO_3$ cubes as an efficient visible-light-driven composite photocatalyst for the degradation of tetracycline and mechanism insight, J. Hazard. Mater. 390 (2020), 122158.
[45] F. Guo, X.L. Huang, Z.H. Chen, H.R. Sun, L.Z. Chen, Prominent co-catalytic e ffect of CoP nanoparticles anchored on high-crystalline g-C_3N_4 nanosheets for enhanced visible -light photocatalytic degradation of tetracycline in wastewater, Chem. Eng. J. 395 (2020), 125118.
[46] H.F. Wang, X. Chen, F. Feng, X. Ji, Y. Zhang, EDTA etching: a simple way for regulating the traps, size and aqueous-dispersibility of Cr^{3+}-doped zinc gallate, Chem. Sci. 9 (2018) 8923–8929.
[47] A. Gulino, F. Lupo, M.E. Fragala, Substrate-free, self-standing ZnO thin films, J. Phys. Chem. C. 112 (2008) 13869–13872.
[48] A. Gulino, I. Fragala, Deposition and characterization of transparent thin films of zinc oxide doped with Bi and Sb, Chem. Mater. 14 (2002) 116–121.
[49] X. Li, S. Zhang, Y. Dang, Z. Liu, Z. Zhang, D. Shan, X. Zhang, T. Wang, X. Lu, Ultratrace naked-eye colorimetric ratio assay of chromium(III) ion in aqueous solution via stimuli-responsive morphological transformation of silver nanoflakes, Anal. Chem. 91 (2019) 4031–4038.